Journal of Hazardous Materials 412 (2021) 125261

Contents lists available at ScienceDirect

Journal of Hazardous Materials

journal homepage: www.elsevier.com/locate/jhazmat

Research Paper

Immobilization and migration of arsenic during the conversion of microbially induced calcium carbonate to hydroxylapatite

Maolin Wang [a,b,c,1], Shijun Wu [a,b,*], Jianan Guo [a,b,c], Zisheng Liao [a,b,c], Yongqiang Yang [a,b], Fanrong Chen [a,b], Runliang Zhu [a,b]

[a] CAS Key Laboratory of Mineralogy and Metallogeny & Guangdong Provincial Key Laboratory of Mineral Physics and Materials, Guangzhou Institute of Geochemistry, Chinese Academy of Sciences, 511 Kehua Street, 510640 Guangzhou, China
[b] CAS Center for Excellence in Deep Earth Science, 511 Kehua Street, 510640 Guangzhou, China
[c] University of Chinese Academy of Sciences, 19 Yuquan Road, 100049 Beijing, China

ARTICLE INFO

Editor: Dr. R. Debora

Keywords:
Arsenic
Immobilization
Mineral conversion
Hydroxylapatite
Microbially induced calcium carbonate precipitation

ABSTRACT

Coprecipitation with calcium carbonate ($CaCO_3$) could decrease the bioavailability of arsenic (As). However, in a phosphate-rich environment, some $CaCO_3$ will be converted to hydroxylapatite (HAP). Currently, the behavior of carbonate-bound As during conversion is unclear. Therefore, we prepared bio-induced $CaCO_3$ in an As solution and converted it to HAP. The results showed that a high concentration of arsenate promoted vaterite precipitation and the conversion of $CaCO_3$ to HAP. The dissolution data verified the low solubility of As in HAP, though its As-bearing $CaCO_3$ precursor released up to 88.19% As during the conversion. Furthermore, HPLC-ICP-MS data showed partial oxidation of arsenite to arsenate, suggesting that $CaCO_3$ and HAP's structure favored the incorporation of arsenate. Our results demonstrated that the stability of heavy metal-bearing $CaCO_3$ should be considered, and the role of HAP in the immobilization of heavy metals such as As should not be overestimated.

1. Introduction

Historically, arsenic (As) was commonly referred to as the 'king of poisons' (Hughes et al., 2011). Ingestion of large doses of soluble inorganic As could bring about gastrointestinal symptoms, disturbances of cardiovascular and nervous system functions, and even death (WHO, 2001; Khairul et al., 2017). Long-term exposure to As by drinking water, air, and food will increase cancer risk in the skin, lungs, bladder, and kidneys (Bates et al., 1992; WHO, 2001; Roy and Saha, 2002). Occupational exposure to As, primarily by inhalation, is usually associated with lung cancer (WHO, 2001; Brüske-Hohlfeld, 2009). Therefore, As is ranked as the No. 1 priority hazardous substance by the *Agency for Toxic Substances and Disease Registry* (ATSDR, 2019).

Arsenic pollution has become a relentless worldwide environmental problem. Significant sources of soil As contamination are coal-fired power generation plants, mining, smelting, agricultural pesticides, and volcanic activity (Garelick et al., 2008; Wang et al., 2019a). Arsenic pollution is closely related to its geochemical behavior in near-surface environments. The interaction between As and minerals via processes such as ion exchange, sorption/desorption, and coprecipitation/dissolution processes can control the environmental behavior of As (Yokoyama et al., 2012). Fe hydroxides are unstable, although they have the highest K_d values for both As(III) and As(V); therefore, they might release As under reducing conditions (Dixit and Hering, 2003). For example, up to 45–50 mg L^{-1} As (Smedley and Kinniburgh, 2002) was desorbed from Fe/Mn oxyhydroxide; it was the dominant source of As contamination in geothermal water and groundwater (Chakraborty et al., 2011; Yokoyama et al., 2012).

Carbonate minerals are potential sinks of heavy metal(loid)s, and the carbonate-bound fraction is one of the most critical forms of heavy metal (loid)s in soil. For example, coprecipitation of the Ca-As complex or As adsorption onto calcite was one of the main processes of As retention on carbonate-rich aquifer materials at Zimapán, Mexico, an As polluted mine site (Romero et al., 2004). Furthermore, As could incorporate into the lattice of calcite via substitution for CO_3^{2-} anions (Di Benedetto et al., 2006; Fernández-Martínez et al., 2006; Román-Ross et al., 2006;

* Corresponding author at: CAS Key Laboratory of Mineralogy and Metallogeny & Guangdong Provincial Key Laboratory of Mineral Physics and Materials, Guangzhou Institute of Geochemistry, Chinese Academy of Sciences, 511 Kehua Street, 510640 Guangzhou, China.
E-mail address: wus@gig.ac.cn (S. Wu).
[1] Present Address: Key Laboratory of Industrial Ecology and Environmental Engineering (Ministry of Education), School of Environmental Science and Technology, Dalian University of Technology, Dalian 116024, China.

https://doi.org/10.1016/j.jhazmat.2021.125261
Received 3 November 2020; Received in revised form 8 January 2021; Accepted 26 January 2021
Available online 29 January 2021

Alexandratos et al., 2007; Bardelli et al., 2011), resulting in As being less available for adsorption on the surface, thereby immobilizing As unless the host phase dissolved (Román-Ross et al., 2006).

Microbially induced calcite or calcium carbonate precipitation (MICP) is a natural phenomenon that widely exists in the environment (Boquet et al., 1973). MICP has recently been developed as a remediation technology for heavy metals (Phillips et al., 2013; Kumari et al., 2016), potentially retarding the migration of As in soil and underground water (Achal et al., 2012). However, a recent study demonstrated that up to 30% of the microbially precipitated calcite dissolved again after 30 days, caused by the pH decrease due to the ammonia volatilization (Gat et al., 2017). The dissolution of carbonate minerals could release trace metals from their crystals, being a source of heavy metals and As (Edmond, 1992; Palmer and Edmond, 1993; Kirsch et al., 2014; Wunsch et al., 2014; Xia et al., 2020).

$CaCO_3$ will alter and convert to hydroxylapatite (HAP) in a phosphate-rich environment because the latter is less soluble than the former (Putnis, 2009). An interesting example is the formation of HAP-containing phosphate guanos on islands and in caves, being the direct product of the reaction between bird or bat guano and calcareous substratum (Schnug et al., 2018; Onac, 2019). In calcareous soil, most phosphate fertilizer will spontaneously transform into HAP, remarkably reducing phosphorus's bioaccessibility (Shen et al., 2011). Furthermore, the formation of HAP occurred on ancient marble buildings (Maravelaki-Kalaitzaki, 2005; Vazquez-Calvo et al., 2006), and coral-based bone implants (Ripamonti et al., 2009). Therefore, conversion-formed HAP can be used for the consolidation of carbonate stones (Sassoni et al., 2011), the conservation of outdoor marble artworks (Sassoni et al., 2015), and bone substitute materials (Neto and Ferreira, 2018).

The chemical composition of hydrothermal apatite could reflect its precursor's composition (Chakhmouradian et al., 2017) and the fluid where it precipitated (Spear and Pyle, 2002; Pedrosa et al., 2016). Borg et al. (2014) have demonstrated that aqueous arsenic can be immobilized by apatite converted from calcite (Liu et al., 2017). As mentioned previously, As can be incorporated into the lattice of calcite (Di Benedetto et al., 2006; Fernández-Martínez et al., 2006; Alexandratos et al., 2007; Bardelli et al., 2011). However, the knowledge on the fate of As trapped in $CaCO_3$ during the $CaCO_3$–HAP replacement reaction under hydrothermal conditions is scarce. Since carbonate minerals are the sink of soil As, during MICP, a question on the stability of carbonate-bound As in the phosphate-rich environment should be discussed. Recently, we reported the immobilization of cadmium (Cd), either incorporated in calcite or an aqueous source, by HAP converted from microbially induced calcite (Wang et al., 2019b). However, Cd and As have different electrical properties and charges, leading to different occupied sites in calcite and apatite. Therefore, one can expect the behavior of As to differ from that of Cd during the conversion of calcite to HAP.

Herein, we provide further evidence of MICP and in situ transformation in the presence of As. This study aims to identify the migration of carbonate-bound As during the conversion of microbially induced calcium carbonate. For comparison, the behavior of aqueous As during the conversion of As-free $CaCO_3$ was also involved.

2. Materials and methods

2.1. Preparation of arsenic-bearing $CaCO_3$

Sporosarcina pasteurii (DSM33, equal to ATCC11859) was supplied by the Guangdong Microbial Culture Collection Center (GDMCC). This bacterial strain was conserved in CASO agar media with the following solid ingredients: 15.00 g L^{-1} casitone, 5.00 g L^{-1} soytone, 15.00 g L^{-1} NaCl, 20.00 g L^{-1} urea, and 20.00 g L^{-1} agar. MICP experiments were carried out in nutrient broth-urea (NBU) media, whose liquid chemicals included 5.00 g L^{-1} peptone, 3.00 g L^{-1} beef extract, 11.10 g L^{-1} $CaCl_2$, and 20.00 g L^{-1} urea. All of the medium except urea were autoclaved at 121 °C for 30 min firstly, then cultured at 30 °C in 500 mL incubator flasks at 150 rpm. The new strain was cultured in a shaker for 24 h, and the microbial density reached more than 10^7 cfu mL^{-1} according to the flat colony counting method. A volume of 1.0 mL of the bacterial suspension was inoculated into a 500 mL flask filled with 200 mL of NBU and cultivated in an incubator shaker (150 rpm) at 35 °C.

As-bearing $CaCO_3$ were prepared and labeled as As(III)-$CaCO_3$ and As(V)-$CaCO_3$ based on the different source, i.e., $NaAsO_2$ or Na_2HAsO_4. Stock solutions containing 10, 50, 100, 250, 500, 1000, and 2000 mg L^{-1} of As(III) or As(V) were added into the flask firstly, and then the cultured bacteria. For comparison, As-free $CaCO_3$ was prepared as well.

2.2. Conversion of $CaCO_3$ to hydroxylapatite

As-$CaCO_3$ was used to study the fate of As incorporated in $CaCO_3$ during its conversion to HAP. For the As-free $CaCO_3$ system, a $NaAsO_2$ or Na_2HAsO_4 stock solution was added to study the fate of aqueous As during the conversion. The main difference between the two systems was the time of As addition. The conversion experiments were performed in the same flask used for MICP. In brief, 3.16 g of solid $(NH_4)_2HPO_4$ was loaded into the flask directly after the precipitation of $CaCO_3$ (96 h after the inoculation of *Sporosarcina pasteurii*) to launch the smooth replacement progress. The molar ratio of phosphate to total calcium was set to 1.2. The temperature of the incubator was 70 °C, and the reaction time was 96 h. Afterward, the suspension was centrifuged at 4000 rpm for 5 min and filtered through a 0.22-μm membrane. The precipitates were dried for further characterization, and the filtrate was collected for chemical analysis. As-bearing HAPs were labeled As(III)-HAP and As(V)-HAP. For clarity, all HAP types and their synthesis information were listed in Table S1. All experiments were conducted in triplicate.

2.3. Phase identification

Powder X-ray diffraction (XRD) patterns were recorded using a Brucker D8 AdvanceX diffractometer (Bruker AXS, German) with a Cu anode (40 kV and 40 mA). Samples were scanned between 3° and 80° (2θ) with a scan speed of 5 °/min and identified based on the ICCD database. The semiquantitative analysis was carried out with Jade 6.5 using RIR values.

2.4. Spectroscopy characterization

Fourier transform infrared spectroscopy (FTIR) spectra were collected by a Brucker Vertex-70 spectrometer between 4000 and 400 cm^{-1}. Sample powders were milled together with KBr at a mass ratio of 1:90 and pressed into a transparent disk for analysis at room temperature.

2.5. Morphology observation

The morphology of the precipitates and the elemental analysis were determined by a field emission scanning electron microscopy (SEM) system (type SU8010) equipped with an energy-dispersive X-ray spectroscopy (EDS) detector (Apollo X-SDD Det) and operated with an accelerating voltage of 1.5 kV. Selected grains were mounted in an epoxy resin and then cut and polished back to their approximate center for microanalysis.

2.6. Stability of arsenic in $CaCO_3$ and hydroxylapatite

Dissolution experiments were performed to evaluate the long-term stability of As in HAP and $CaCO_3$. Five types of samples were studied, including As-HAP converted from As-$CaCO_3$ (labeled A1 and A6), As-HAP converted from pure $CaCO_3$ reacted in As solution (labeled A2 and A7), As-$CaCO_3$ (labeled A3 and A8), microbe precipitated pure $CaCO_3$ after adsorption of As (As-adsorbed $CaCO_3$, labeled A4 and A9),

and HAP converted from pure $CaCO_3$ after adsorption of As (As-adsorbed HAP, labeled A5 and A10). As(III) and As(V) were used to prepare the A1–A5 and A6–A10 samples, respectively. The loaded As in each sample was 1044.79, 1011.33, 1057.46, 1276.79, and 1093.66 mg kg^{-1} for A1–A5, and 1165.82, 1126.09, 963.45, 1108.07, and 986.47 mg kg^{-1} for A6–A10, respectively (Table S2). A 500 mg sample and a 5 mL solution with pH values of 2.0, 7.0, and 10.0 were loaded into a 15 mL polypropylene centrifuge tube. The used solution was prepared using ultrapure water, and the pH was adjusted using HNO_3 and NaOH solution. The tubes were capped and placed in an overhead shaker (40 rpm) and kept at a temperature of 25 °C for seven days. Afterward, the supernatant was filtered using a 0.22 μm pore diameter membrane, diluted with 0.2% HNO_3, and then analyzed. All dissolution experiments were performed in triplicate.

2.7. Measurement of the arsenic concentration

Both the liquid media and precipitates were digested by microwave using 5 mL of HNO_3 (14.4 mol L^{-1}) and 1 mL of H_2O_2 (30% in volume) to eliminate the effect of organic materials. After that, the concentration of As in the liquid was analyzed by inductively coupled plasma atomic emission spectroscopy (ICP-AES, Varian Vista-Pro) and inductive coupled plasma mass spectrometry (ICP-MS, Thermo Scientific-iCAP Qc).

2.8. Valence characterization

The As valence state was characterized according to Yokoyama et al. (2012). As-$CaCO_3$ and As-HAP were dissolved in 37% hydrochloric acid. The obtained supernatant was softened using a cation exchange resin and then filtered through a 0.22 μm membrane. The contents of As(III) and As(V) were characterized through high-performance liquid chromatography inductive coupled plasma mass spectrometry (HPLC-ICP-MS) (Agilent 1260; Thermo Fisher ICAP Qc). The mobile phase was an aqueous solution containing 30 mM NH_4HCO_3 at pH 7.9, in which As(III) and As(V) were segregated as H_3AsO_3 and $HAsO_4^{2-}$, respectively. The flow velocity of the fluid phase was 1.0 mL min^{-1}. 100 mL of ultrapure water was injected into the chromatographic system between the measurements to remove any remaining As in the inlet and syringe solution.

3. Results and discussion

3.1. XRD and FTIR characterization

In the absence of As, the white precipitate collected four days after *Sporosarcina pasteurii* was introduced into the NBU medium was identified as calcite by XRD (Fig. 1, S1a). Besides, calcite was confirmed as the only crystalline product in the presence of 10–2000 mg L^{-1} aqueous As(III) and 10–50 mg L^{-1} aqueous As(V) (Fig. 1, S1). Interestingly, the XRD patterns showed additional reflections at 24.9, 27.0, and 32.7° in the presence of 100–2000 mg L^{-1} As(V), suggesting the appearance of vaterite. Semiquantitative calculations indicated that 5%, 11%, 38%, 64% and 100% vaterite was produced at initial As(V) concentrations of 100, 250, 500, 1000, and 2000 mg L^{-1}, respectively (Fig. 1, S1b). Linear fitting showed that the fraction of vaterite was positively correlated with the initial concentration of As(V) range from 100 to 2000 mg L^{-1}, with an R^2 value of 0.96 (Fig. S2).

After 96 h of conversion was performed for As(III)-$CaCO_3$, the typical XRD patterns showed intense reflections at 31.8°, which corresponded to the (211) plane of the HAP structure (Figs. 1, S3a). In most cases, there was trace unreacted calcite. The semiquantitative calculation showed that the fraction of HAP in products was over 96% when the initial As(III) concentrations were above 500 mg L^{-1}. Comparably, the fraction of HAP was 79–83% when the initial As(III) concentration was below 500 mg L^{-1} (Figs. S4, S5a). A similar HAP fraction distribution

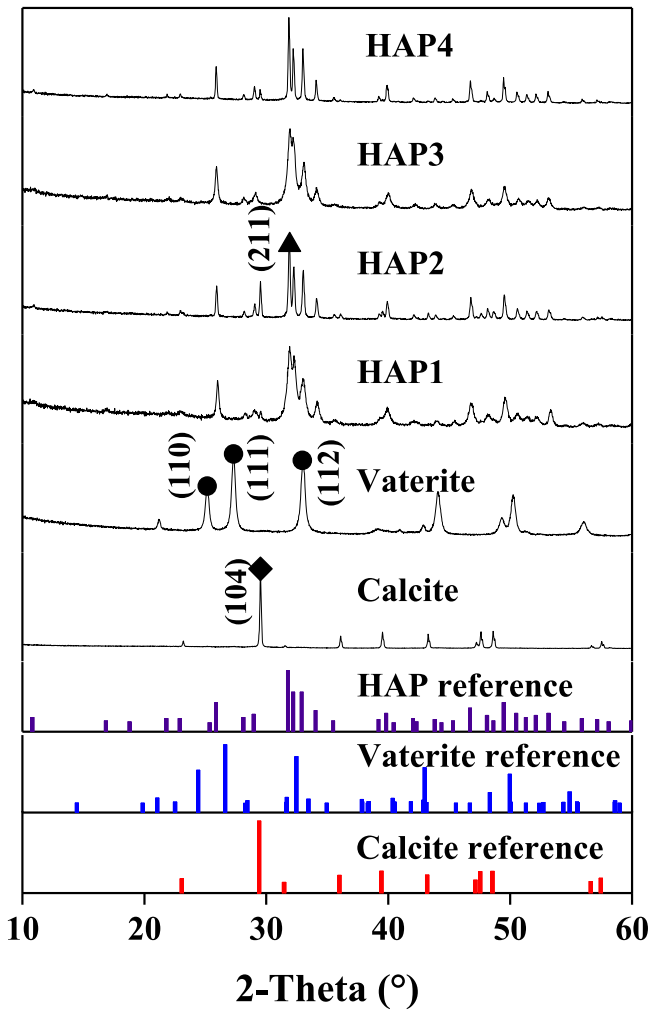

Fig. 1. Typical powder XRD patterns of microbially precipitated $CaCO_3$ and its converted hydroxylapatite. (Reference data for calcite, vaterite, and hydroxylapatite were obtained from the ICDD database with code numbers 01-072-1937, 01-74-1867 and 01-089-6437. HAP1 refers to HAP converted from As (III)-Calcite; HAP2 refers to HAP converted from As-free calcite in As(III) solution; HAP3 refers to HAP converted from As(V)-vaterite; HAP4 refers to HAP converted from As-free calcite in As(V) solution; Calcite refers to the product of microbially induced $CaCO_3$ precipitation in As(III) solution; and vaterite refers to the product of microbially induced $CaCO_3$ precipitation in As(V) solution. The initial concentration of As was 2000 mg L^{-1}.)

was displayed for the As(V)-HAP converted from As(V)-$CaCO_3$ (Figs. S4, S5a) but not for the HAP converted from As-free $CaCO_3$ (Figs. S4, S5b). This result showed that the incorporation of As in $CaCO_3$ promoted the formation of HAP. Meanwhile, the fraction of HAP converted from As (V)-$CaCO_3$ was higher than that from As(III)-$CaCO_3$, probably due to the smaller particle size and more significant surface area of vaterite than calcite. Furthermore, the diffraction peaks of the generated HAP became wider and blunter with increasing initial As concentrations, indicating a high As concentration yielded HAP with low crystallinity (Fig. S3).

Typical FTIR spectra are shown in Fig. 2, S6-S7. Two sharp peaks at 870 and 1440 cm^{-1} and two weak peaks at 713 and 1043 cm^{-1} were assigned to the υ_3, υ_2, υ_1, and υ_4 bands of calcite. The split peaks at approximately 1490 and 1420 cm^{-1} (Fig. 2, S6) shifted υ_4 from 715 to 750 cm^{-1}, indicating vaterite structure (Andersen et al., 1991; Sato and Matsuda, 1969). Usually, vaterite is metastable when exposed to water because it can rapidly transform to aragonite within 60 min at 60 °C and recrystallize to calcite within 20–24 h at room temperature (Grasby, 2003). However, vaterite (biogenic and abiogenic) is often observed

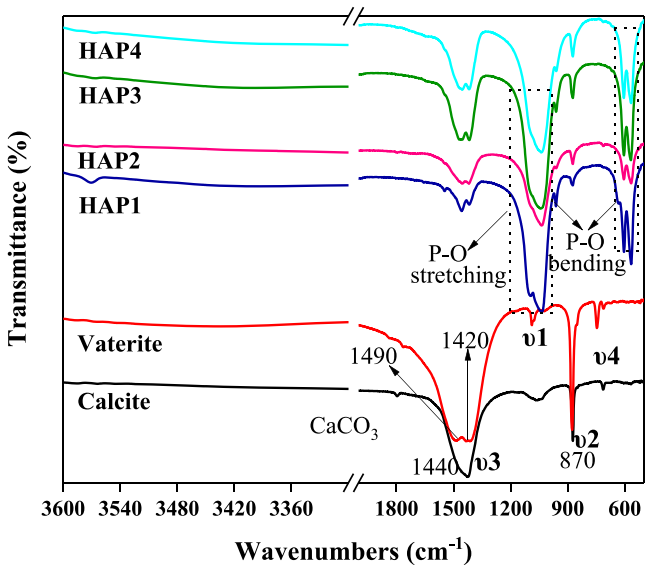

Fig. 2. FTIR spectra of microbially precipitated $CaCO_3$ and its converted hydroxylapatite. (All sample information is the same as that shown in Fig. 1.)

together with calcite in the presence of impurities such as AsO_3^{3-} (Achal et al., 2012; Román-Ross et al., 2006), SeO_4^{2-} (Fernandez-Gonzalez and Fernandez-Diaz, 2013), CrO_4^{2-} (Sanchez-Pastor et al., 2011), SO_4^{2-} (Fernandez-Diaz et al., 2010), Co^{2+} (Katsikopoulos et al., 2008), and La^{3+} (Kamiya et al., 2004). Meanwhile, Yokoyama et al. (2012) reported that both As(III) and As(V) stabilized vaterite up to 24 h. Therefore, the occurrence of vaterite is time, and impurities depended. Our observation of pure vaterite indicated that As(V) could promote the stability of vaterite much better than As(III) and delay its transformation to calcite.

After conversion, the FTIR spectra showed that the products were typical carbonated apatite, similar to our previous investigation (Wang et al., 2019b). There was no residual vaterite in HAP3, according to the XRD data. Therefore, the split peaks at 1420 and 1453 cm^{-1} confirmed phosphate substitution by carbonate (type B apatite) (Fleet and Liu, 2008). The peaks at ~870, 1453, and 1420 cm^{-1} could be assigned to carbonate in apatite and residual calcite/vaterite.

3.2. *Arsenic immobilization by $CaCO_3$*

According to the ICP-MS/AES data, As concentrations in As(III)-$CaCO_3$ were 76.93 and 285.09 mg kg^{-1} when the initial As concentrations were 10 and 50 mg L^{-1}, respectively, which were higher than those in As(V)-$CaCO_3$ (64.58 and 277.23 mg kg^{-1}) (Fig. 3a, Table S3). Nevertheless, this trend reversed with initial As concentrations rising from 100 to 2000 mg L^{-1}, especially, 564.59–26,027.47 mg kg^{-1} versus

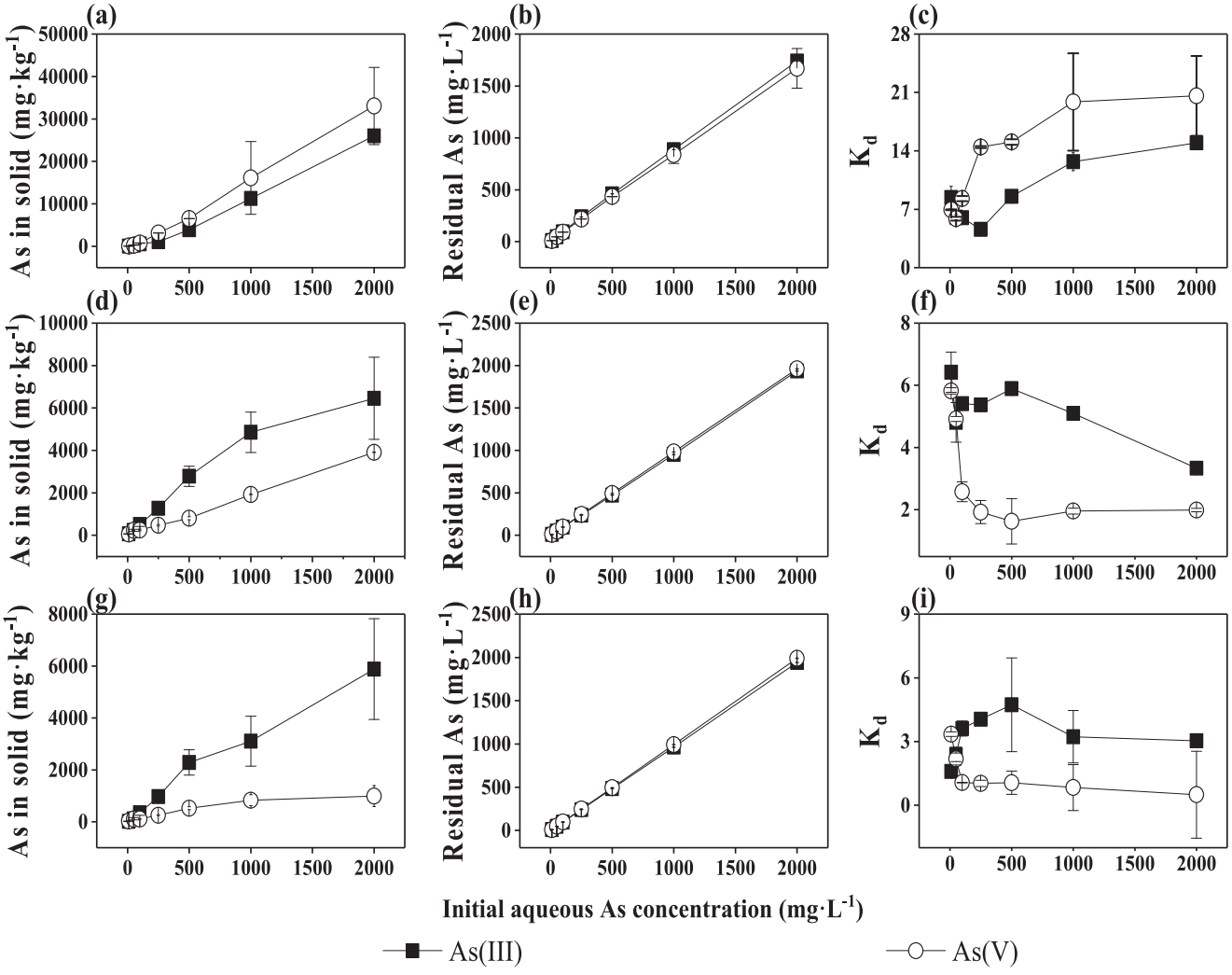

Fig. 3. Variations in As concentration in microbially precipitated $CaCO_3$ and its converted hydroxylapatite. (a–c, microbially induced calcium carbonate precipitation; d–f, HAP converted from As-$CaCO_3$; g–i, HAP converted from As-free $CaCO_3$ in As solution.)

764.60–33,073.02 mg kg^{-1} of As in As(III)-$CaCO_3$ and As(V)-$CaCO_3$, respectively (Table S3). Meanwhile, the residual aqueous As concentration varied from 9.23–1739.72 mg L^{-1} for As(III) and 9.30–1669.27 mg L^{-1} for As(V), resulting in corresponding removal efficiencies of 7.7–13.0% and 7.0–16.5%, respectively (Table S3). The vaterite percentage has increased from 11% to 100% as the As concentration increased from 100 to 2000 mg L^{-1}. Further calculations showed that the As concentrations in As(V)-$CaCO_3$ is positively correlated with the proportion of vaterite, with an R^2 value of 0.957 ($y = 327.64x - 2350.6$, $5 \leq x \leq 100$).

At the initial As of 2000 mg L^{-1}, As concentration in As(V)-vaterite (33,073.02 mg kg^{-1}) was 1.27 times than that in As(III)-calcite (26,027.47 mg kg^{-1}) (Table S3). These data suggested that the vaterite structure could tolerate As(V) better than calcite could tolerate As (III). Currently, the mechanism responsible for vaterite preferring As(V) is not yet known. Based on the structural comparison, it is most likely that the substitution of disordered carbonate within vaterite (Christy, 2017) by tetragonal arsenate is more accessible than that by arsenite. However, further investigation is necessary to obtain a better understanding of the mechanism.

Note that a white product precipitated immediately as 2000 mg L^{-1} As(V) was added into the NBU medium, consuming 81.89% Ca^{2+} and 83.75% As(V) (Fig. 4a). XRD data demonstrated that the white precipitate was mainly composed of calcium arsenate and its hydrates (Fig. S8). Calcium arsenate formation is a widely used As immobilization method to treat As-containing wastewater (Bothe and Brown, 1999). However, there was no visible precipitate at the early stage when 100 mg L^{-1} or less As(V) was used, possibly due to organic compounds in the system. Detailed kinetic analysis showed that the aqueous As amount increased again while the aqueous calcium was depleted during the MICP process (Fig. 4a). As releasing and vaterite's occurrence suggest that the initially precipitated calcium arsenate has transformed to vaterite via the dissolution-precipitation mechanism (Juillot et al., 1999). Under atmospheric conditions, a long-term stability investigation revealed that calcium arsenate would transform into various types of crystalline calcium carbonates, i.e., calcite, aragonite, vaterite, monohydrocalcite, and ikaite (Zhang et al., 2019). In our experiment, abundant CO_3^{2-} produced with the growth of microbe and hydrolysis of urea, which accelerated the transformation of calcium arsenate.

To further understand the transformation of calcium arsenate, the initial precipitate was separated and added into fresh media without Ca^{2+}. The increase in the aqueous calcium and As concentrations demonstrated the dissolution of calcium arsenate at the early stage (0–12 h) (Fig. 4b). After that, vaterite precipitated together with the further release of As (12–96 h). The maximum aqueous calcium concentration was only 8.23 mg L^{-1}, indicating that most dissolved calcium precipitated immediately at the calcium arsenate surface and was not released to the water body.

3.3. Arsenic immobilization by As-HAP

After 96 h of conversion was performed in a phosphate solution, As concentrations in the solution increased 0.16–195.75 mg L^{-1} (As(III)) and 0.15–291.67 mg L^{-1} (As(V)), with As removal efficiencies of 6.0–3.2% and 5.5–2.0%, respectively (Table S3). These data demonstrated that As(III)-$CaCO_3$ released 9.1–75.2% of the trapped As during the conversion, while As(V)-$CaCO_3$ released 15.5–88.2% (Fig. 3e). Accordingly, the converted As-HAP from As-$CaCO_3$ possessed As concentrations of 60.46–6452.07 mg kg^{-1} (As(III)) and 54.96–3906.08 mg kg^{-1} (As(V)), respectively (Fig. 3d, Table S3). Figs. S9a and S10a show the remarkable decline in the As concentrations in solids converted from As-$CaCO_3$ to As-HAP. On the other hand, the As-HAP converted from As-free $CaCO_3$ possessed As concentrations of 22.20–5885.09 mg kg^{-1} for As(III)-HAP and 21.83–991.72 mg kg^{-1} for As(V)-HAP (Fig. 3g). For comparison, the As-HAP converted from As-$CaCO_3$ contained more As than that converted from As-free $CaCO_3$ at the same initial As concentration, which was similar to Cd's immobilization by HAP (Wang et al., 2019b).

3.4. Morphology of As-$CaCO_3$ and As-HAP

According to our previous study, the As-free NBU medium-precipitated calcite was composed of aggregates of smaller particles with a rhombohedral, spheroidal, or dipyramidal morphology (Wang et al., 2019b). With the increase in initial As(III) concentrations, the spherical aggregates gradually disappeared, and the rhombic aggregates

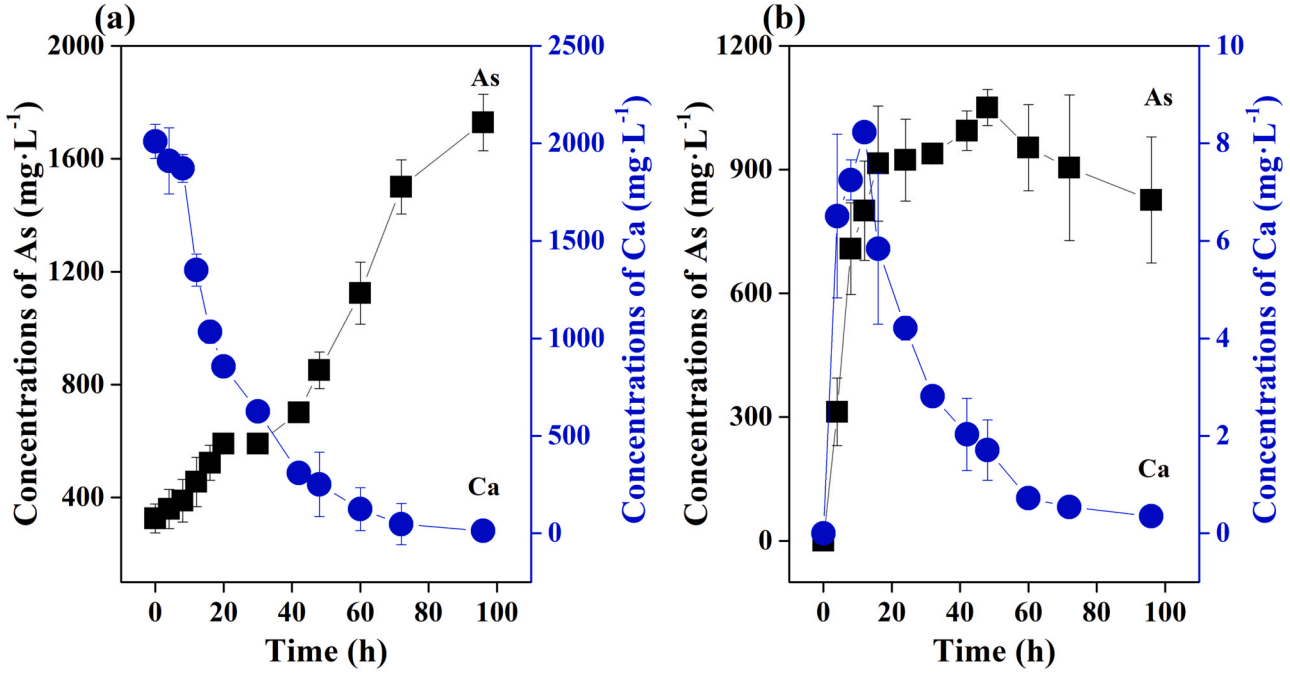

Fig. 4. Kinetic evolution of aqueous As and Ca concentrations during the MICP process. (a, 2000 mg L^{-1} As(V) was induced before the microbe; b, The separated precipitate shown in Fig. S8 was added into the fresh medium without Ca^{2+}.)

gradually became a preponderant single rectangular accumulation. When the initial As(III) concentration was 2000 mg L^{-1}, the obtained calcite crystals became small particles with rod aggregates (Fig. 5a–c) due to the c-axis elongation of the rhombohedral calcite crystals. This morphology variation suggested that As(III) incorporation could induce a change in the crystal growth direction. The most apparent change in the $CaCO_3$ morphology was the occurrence of spherical vaterite in the presence of As(V) (Fig. 5e and f). With low concentrations of As(III) and As(V), As-$CaCO_3$ was a rhombohedral crystal. When the initial concentration of As(V) increased to 250 mg L^{-1}, the precipitate was an agglomeration of rhombohedral and spherical particles (Fig. 5d and e). However, the nano-ellipsoidal small particles that appeared on the surface of vaterite piled up with a particular order at 2000 mg L^{-1} As(V) (Fig. 5f) and consisted predominantly of a hexagonal structure with at least another coexisting nanodomain structure (Kabalah-Amitai et al., 2013). This observation indicated that the incorporation of oxyanions such as AsO_4^{3-} could change the crystal morphology and cause aggregation/agglomeration during the growth of $CaCO_3$ polymorphisms (Sanchez-Pastor et al., 2011; Fernandez-Gonzalez and Fernandez-Diaz, 2013). As shown in Fig. 5g and j, when trace As was present in the precursor calcite, the obtained HAP showed the same perfect prismatic hexagonal morphology as As-free HAP morphology. With more As loading, the obtained HAP showed subhedral, bipyramidal, or spindle-shaped crystals where the face edges became rounded (Fig. 5h). However, HAP's morphology changed to trivial tabular at an initial As concentration of 2000 mg L^{-1}(Fig. 5i). Comparably, tabular-like HAP with a thickness of ~100 nm formed at 250 mg L^{-1} As(V) and changed to a petal-like morphology with a thickness of ~20 nm at 2000 mg L^{-1}

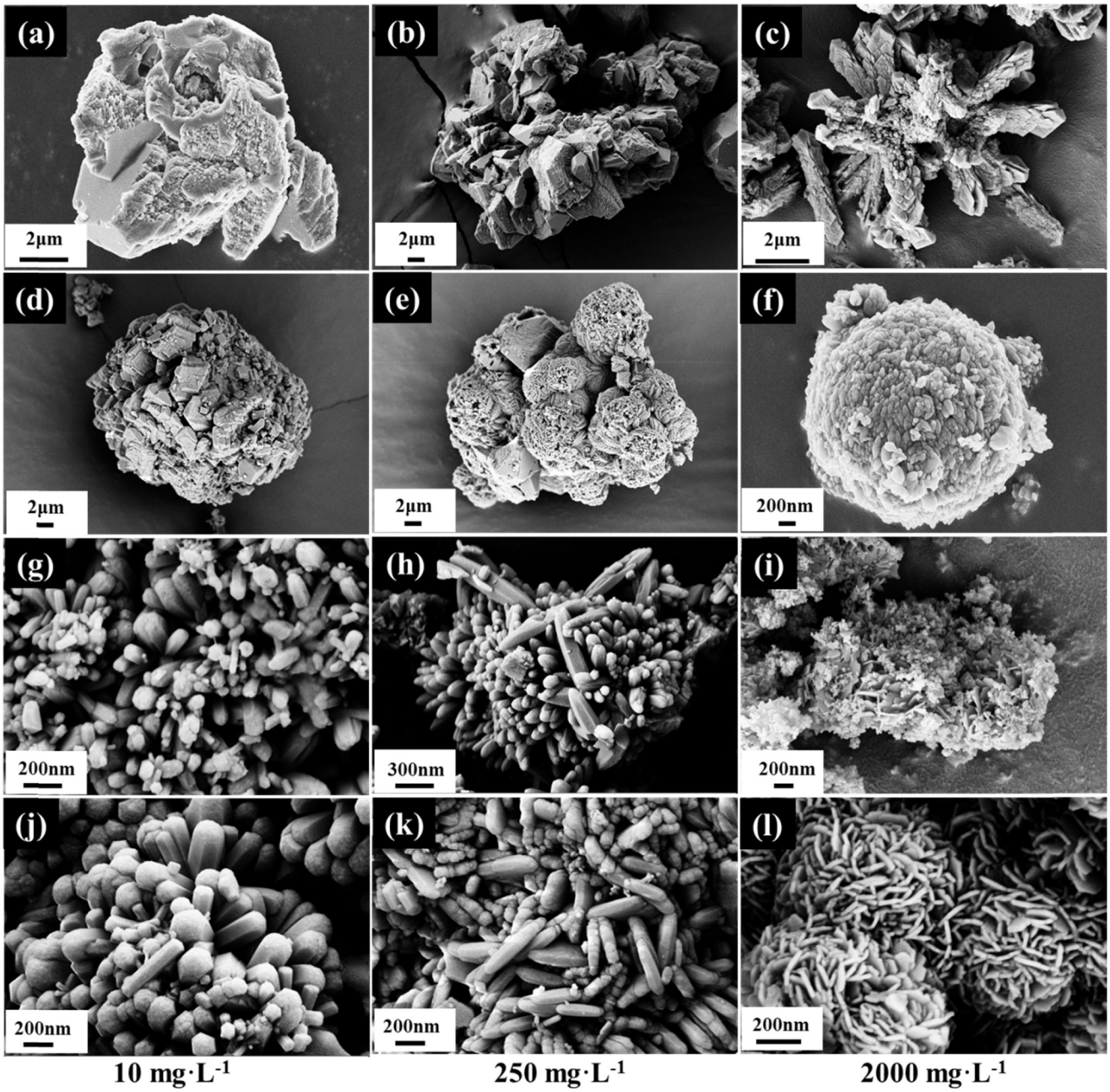

Fig. 5. SEM images of microbially precipitated $CaCO_3$ and its converted hydroxylapatite. (a–c, As(III)-$CaCO_3$; d–f, As(V)-$CaCO_3$; g–i, As-HAP converted from As(III)-$CaCO_3$; j–l, As-HAP converted from As(V)-$CaCO_3$; initial As concentrations were 10 mg L^{-1}, 250 mg L^{-1}, and 2000 mg L^{-1}.)

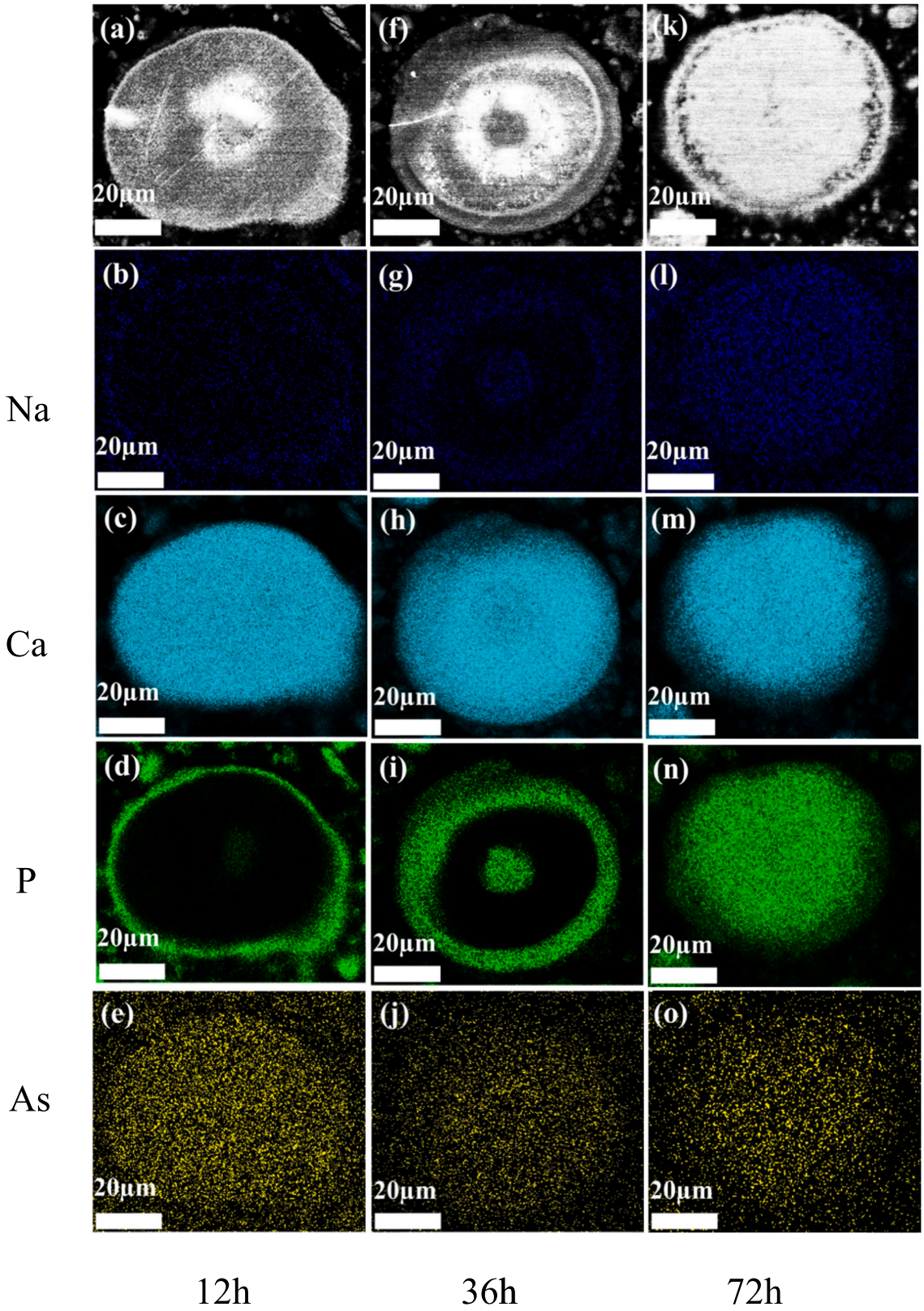

Fig. 6. Elemental mapping of selected polished samples after As-vaterite was converted at 12, 36, and 96 h in aqueous phosphate. (a–e, 12 h; f and g, 36 h; k–o, 96 h. The initial concentration of As(V) was 2000 mg L^{-1}.).

As(V) (Fig. 5j–l). When As was added after the precipitation of $CaCO_3$, the obtained As-HAP appeared as prismatic hexagonal without a change in the morphology (Fig. S11). This observation suggested that impurities such as Cd and As in the $CaCO_3$ precursor could control the obtained HAP crystal growth and habits (Wang et al., 2019b).

3.5. The distribution of arsenic in $CaCO_3$ and HAP

Fig. 6 showed the selected polished samples' elemental map after As-vaterite was converted at 12, 36, and 96 h. At the early stage of conversion (12 h), phosphorus appeared only at the crystal's outer surface (Fig. 6d). With the continuing conversion, phosphorus gradually entered the core (Fig. 6i and n). The change in the phosphorus distribution in a single crystal agreed well with the evolution of mineral phases shown in Fig. S12, supporting the conversion pathway from the surface to the core. Meanwhile, sodium distribution showed the same trend as phosphorus, suggesting that sodium was incorporated into the structure of newly precipitated HAP (Fig. 6b, g, and l). Sodium is well known to be a common minor constituent of natural calcium phosphate apatites and many synthetic apatites and has a strong preference for the Ca1 sites (Pan and Fleet, 2002). However, calcium was distributed uniformly in vaterite and apatite (Fig. 6c, h, and m), while vaterite lost some As during conversion (Fig. 6e, j, and o), which was consistent with the ICP data (Section 3.3, Fig. S10a and S10c).

Similar to Ca, P, and Na, As was homogeneously distributed in As-HAP converted from pure calcite in the As-containing phosphate solution (Fig. S13). Comparably, most of the Cd was distributed in the outer surface when pure calcite reacted with the Cd-containing (2000 mg L^{-1}) phosphate solution (Wang et al., 2019b). The different distributions of As and Cd might be attributed to their different lattice sites in HAP (will be discussed later).

3.6. The oxidation state of arsenic

XPS results showed that the B-type apatite absent of As has a C/P molar ratio of 0.50, which decreased to 0.17, 0.38, 0.25, and 0.34 after As doping (Fig. 7a), indicating the competitive substitution of PO_4^{3-} by AsO_4^{3-}/AsO_3^{3-} and CO_3^{2-}. Meanwhile, the P/Ca molar ratio decreased from 0.73 to 0.71, 0.63, 0.69, and 0.67.

We tried to analyze the oxidation state of As using XPS, which showed similar peak binding energies and was therefore not applicable in our samples. However, HPLC-ICP-MS measurements provided useful data on the As(III)/As(V) ratios in the acid-dissolved precipitates. Herein, 36.5% of the total As in As(III)-calcite was As(V) (Fig. 7b), revealing the partial oxidation of As(III) during incorporation. Yokoyama et al. (2012) and Renard et al. (2015) also reported the partial oxidation of As(III) before it was incorporated into calcite, resulting in calcite containing up to 64% As(V). Thus, we proposed that the preferential uptake of As(V) by the calcite structure could drive the oxidation of As(III), no matter in the absence (Yokoyama et al., 2012; Renard et al., 2015) or presence of microbes (this study), resulting in higher As content in As(V)-vaterite than in As(III)-calcite (Section 3.2).

After conversion, the proportion of As(V) in As-HAP (HAP1) increased to 56.0%, suggesting further oxidation of As(III) during conversion. However, only 33.7% of As(III) changed to As(V) with As incorporation into As-HAP (HAP2), as the product of As-free calcite reacted with the As(III)-containing phosphate solution (Fig. 7b). In the study of Liu et al. (2017), only As(III) substitution occurred in the obtained apatite when As(III) was present in the fluid, indicating no As(III) oxidation occurred during conversion, which is different from our results. The partial oxidation of As(III) during conversion in our experiment could be attributed to the different reaction temperatures and times, the presence of microbes and their extracellular polymeric substances (EPS), and the chemicals contained in the nutrient broth-urea (NBU) medium. Furthermore, Liu et al. observed the preferential uptake of As(V) versus As(III) by the apatite structure in mixed As(III)/As(V) experiments (Liu et al., 2017). As shown in Section 3.2, some As was released from calcite during conversion. Therefore, if more As(III) was released than As(V), the obtained HAP1 should possess more As(V) than As(III).

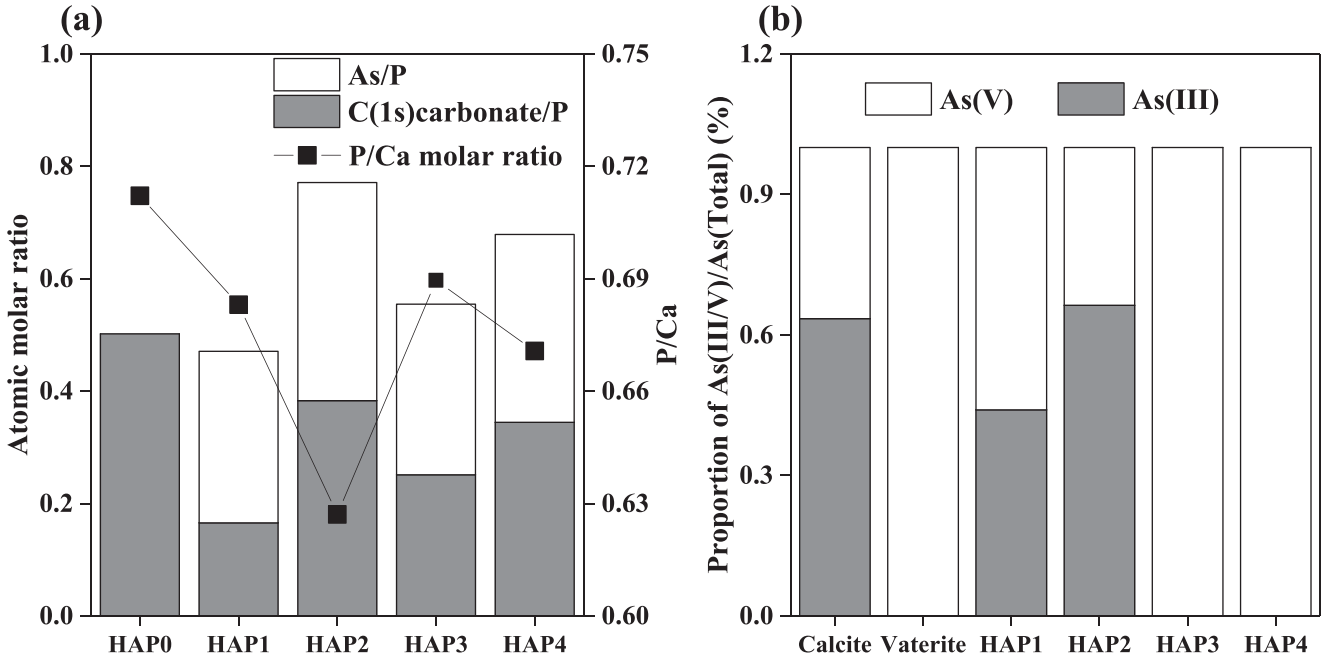

Fig. 7. The atomic molar ratio of HAP obtained from XPS (a) and the valance state of As based on HPLC-ICP-MS (b). (HAP0 refers to HAP converted from As-free $CaCO_3$; HAP1 refers to HAP converted from As(III)-calcite; HAP2 refers to HAP converted from As-free $CaCO_3$ in As(III) solution; HAP3 refers to HAP converted from As(V)-vaterite; HAP4 refers to HAP converted from As-free $CaCO_3$ in As(V) solution; Calcite refers to the product of microbially induced $CaCO_3$ precipitation in As(III) solution; vaterite refers to the product of microbially induced $CaCO_3$ precipitation in As(V) solution. The initial concentrations of As were 2000 mg L^{-1}.).

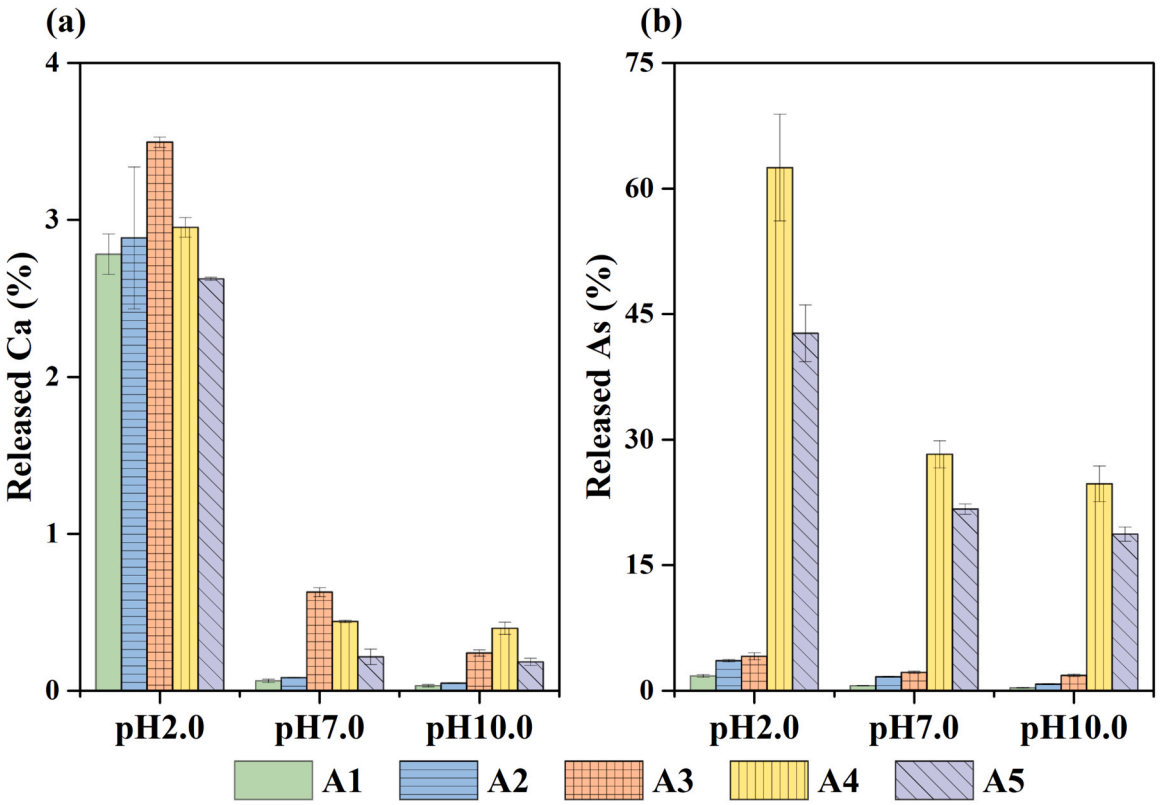

Fig. 8. Release of As(III) during the dissolution of calcite and HAP. (A1 refers to As-HAP converted from As-calcite; A2 refers to As-HAP converted from As-free calcite in As solution; A3 refers to As-calcite; A4 refers to As-adsorbed calcite; A5 refers to As-adsorbed HAP. The original As concentrations in the solids were 1044.79, 1011.38, 1057.46, 1276.79, and 1093.66 mg kg^{-1} for A1 to A5, respectively. As(III) was used in all experiments.)

In the As(V) experiments, only As(V) was observed in vaterite, HAP3, and HAP4, which agreed well with the previous investigation (Liu et al., 2017).

3.7. Leaching of arsenic

After dissolution in an acidic solution, calcite dissolved 3.50% of the calcium, and all HAP dissolved 2.62–2.95% of the calcium (Fig. 8a). Comparably, 1.78% of As was released from A1, while 3.59% and 4.13% of As was released from A2 and A3, respectively (Fig. 8b). Therefore, the conversion of As(III)-$CaCO_3$ to As(III)-HAP indeed reduced the release risk of arsenite by up to 56.9%. Meanwhile, the proportion of As released from A2 was 2.02 times that of A1, indicating that the As in As(III)-HAP that converted from As(III)-$CaCO_3$ was less soluble than that in As(III)-HAP that converted from As-free $CaCO_3$ in As solution. Furthermore, A5 (As(III)-adsorbed HAP) released 42.7%, 21.71%, and 18.70% of the previously adsorbed As at pH 2.0, 7.0, and 10.0, respectively. Comparably, As(III)-HAP released much less As, e.g., 1.78% for A1 and 3.59% for A2, at an initial pH 2.0. Similarly, A4 (As(III)-adsorbed calcite) released 62.50%, 28.26%, and 24.73% of the adsorbed As at pH 2.0, 7.0, and 10.0, while A3 released 4.13%, 2.20%, and 1.84% As, respectively. Our dissolution data revealed that As contained in calcite and the apatite structure is less soluble than the adsorbed As. Therefore, the leachability and bioaccessibility of As followed the trend of A4 > A5 > A3 > A2 > A1. A similar trend was also observed for the As (V) samples, i.e., A9 > A10 > A8 > A7 > A6 (Fig. S14).

3.8. Mechanism of arsenic immobilization and migration

During the process of bacterium-facilitated calcite precipitation (Eq. (1)), As(III) could coprecipitate with CO_3^{2-} to form a solid solution of $Ca(HAsO_3)_x(CO_3)_{(1-x)}$ via substitution (Eq. (2)) (Román-Ross et al., 2006). Alternatively, Na^+ could substitute for Ca^{2+} to maintain the charge balance (Eq. 3). Since the oxidation state of As controlled the species of coprecipitation products and the removal efficiency of As. For example, calcium arsenate precipitated immediately once 2000 mg L^{-1} As(V) entered the NBU medium (Fig. S8, Eq. (4)). With increasing As(V) concentrations, more vaterite and a higher As removal efficiency occurred via the dissolution of calcium arsenate (Eq. (5)) and precipitation of As(V)-$CaCO_3$ (Eqs. (6) and (7)). When As-$CaCO_3$ was soaked in a phosphate solution, the partial dissolution of $CaCO_3$ and subsequently, overgrowth of carbonated HAP occurred, resulting in the partial release of arsenate into the solution and sodium incorporation, as confirmed by EDS mapping (Fig. 6 and Eqs. (8) and (9)). For As-free $CaCO_3$, a two-stage reaction process has been proposed to describe As-HAP formation based on single calcite crystals reacting with aqueous arsenate-phosphate solutions (Borg et al., 2014). (1) On a time scale of hours, $CaCO_3$ dissolved first and was subsequently replaced by compositionally heterogeneous apatite with As enriched in the $CaCO_3$-HAP reaction-interface (Fig. 6a–j, S12a–f) (Borg et al., 2014). (2) The heterogeneous apatite evolved into homogeneous apatite with the extended time through interface-coupled dissolution-precipitation (Fig. 6k–o, S12g–l) (Borg et al., 2014). Therefore, both As(V) and As(III) could be incorporated into HAP with the substitution of CO_3^{2-}/PO_4^{3-} by AsO_3^{3-}/AsO_4^{3-} during recrystallization (Eqs. (10) and (11)). Furthermore, it has been proposed that the high strain on the lattice of HAP caused by $As(III)O_3^{3-}$ moieties replacing phosphate groups resulted in easy oxidization of As(III) to As(V) in the mineral lattice (Liu et al., 2017). The extended X-ray absorption fine structure (EXAFS) confirmed that the size of As-centered tetrahedra remains constant across the solid-solution series (Lee et al., 2009). Though K_{sp} increased from $10^{-57.90}$ for $Ca_5(PO_4)_3OH$ to $10^{-39.22}$ for $Ca_5(AsO_4)_3OH$ (Puzio et al., 2018), the solid solution formed via the substitution of As for phosphorus in the apatite structure is more stable than in calcite

(3.4×10^{-9}).

$$Ca^{2+} + CO_3^{2-} \rightleftharpoons CaCO_3 \quad (1)$$

$$Ca^{2+} + (1-x)CO_3^{2-} + xHAsO_3^{2-} \rightleftharpoons Ca(HAsO_3)_x(CO_3)_{(1-x)} \quad (2)$$

$$(1-x)Ca^{2+} + xNa^{+} + (1-y)CO_3^{2-} + yAsO_3^{3-} \rightleftharpoons Ca_{(1-x)}Na_x(AsO_3)_y(CO_3)_{(1-y)} + (x+y)e^{-} \quad (3)$$

$$3Ca^{2+} + 2AsO_4^{3-} \rightleftharpoons Ca_3(AsO_4)_2 \quad (4)$$

$$Ca_3(AsO_4)_2 \rightleftharpoons 3Ca^{2+} + 2AsO_4^{3-} \quad (5)$$

$$Ca^{2+} + (1-x)CO_3^{2-} + xHAsO_4^{2-} \rightleftharpoons Ca(HAsO_4)_x(CO_3)_{(1-x)} \quad (6)$$

$$(1-x)Ca^{2+} + xNa^{+} + (1-x)CO_3^{2-} + xAsO_4^{3-} \rightleftharpoons Ca_{(1-x)}Na_x(AsO_4)_x(CO_3)_{(1-x)} + 2xe^{-} \quad (7)$$

$$\begin{aligned} &10Ca(HAsO_3)_x(CO_3)_{(1-x)} + (6-y-z)HPO_4^{2-} + \alpha Na^{+} \\ &\quad + (8-z)OH^{-} \rightleftharpoons Ca_{(10-\alpha)}Na_\alpha(PO_4)_{6-y-z}(AsO_3)_y(CO_3)_z(OH)_2 \\ &\quad + \alpha Ca^{2+} + (10x-y)HAsO_3^{2-} + (10-10x-z)CO_3^{2-} + (6-z)H_2O \\ &\quad + (\alpha-z)e^{-} \end{aligned} \quad (8)$$

$$\begin{aligned} &10Ca(HAsO_4)_x(CO_3)_{(1-x)} + (6-y-z)HPO_4^{2-} + \alpha Na^{+} \\ &\quad + (8-z)OH^{-} \rightleftharpoons Ca_{(10-\alpha)}Na_\alpha(PO_4)_{6-y-z}(AsO_4)_y(CO_3)_z(OH)_2 \\ &\quad + \alpha Ca^{2+} + (10x-y)HAsO_4^{2-} + (10-10x-z)CO_3^{2-} \\ &\quad + (6-z)H_2O + (\alpha-z)e^{-} \end{aligned} \quad (9)$$

$$\begin{aligned} &10CaCO_3 + (6-x-y)HPO_4^{2-} + yAsO_3^{3-} + zNa^{+} \\ &\quad + (8-x-y)OH^{-} \rightleftharpoons Ca_{(10-z)}Na_z(PO_4)_{6-x-y}(CO_3)_x(AsO_3)_y(OH)_2 \\ &\quad + (10-x)CO_3^{2-} + (6-x-y)H_2O + zCa^{2+} + (z-x)e^{-} \end{aligned} \quad (10)$$

$$\begin{aligned} &10CaCO_3 + (6-x-y)HPO_4^{2-} + yHAsO_4^{2-} + zNa^{+} \\ &\quad + (8-x)OH^{-} \rightleftharpoons Ca_{(10-z)}Na_z(PO_4)_{6-x-y}(CO_3)_x(AsO_4)_y(OH)_2 \\ &\quad + (10-x)CO_3^{2-} + (6-x)H_2O + zCa^{2+} + (z-x)e^{-} \end{aligned} \quad (11)$$

3.9. Implications

The behavior of As in soil is very complex, which depends on As chemical species and soil chemical properties, such as the soil pH, redox conditions, and organic and inorganic matter (Sadiq, 1997; Redman et al., 2002; Wilson et al., 2010). As one of the most common carbonate minerals, calcite might be present in the soil as the primary and secondary mineral (Bronick and Lal, 2005). It is well known that As can be immobilized via adsorption and coprecipitation with calcite (Di Benedetto et al., 2006; Fernández-Martínez et al., 2006; Román-Ross et al., 2006; Alexandratos et al., 2007; Bardelli et al., 2011; Achal et al., 2012). However, carbonate-bound metals might be released into the environment once calcite dissolves, serving as a heavy metal source (Kirsch et al., 2014; Wunsch et al., 2014). In a phosphate-riched environment, calcite could spontaneously convert to hydroxylapatite and capture As from fluid (Shen et al., 2011; Borg et al., 2014; Liu et al., 2017), resulting in As immobilization. Herein, we reported a significate release of As during the transformation of As-$CaCO_3$ to HAP, suggesting a possible new pollutant source of As in the environment. Although HAP could remove As via adsorption (Sneddon et al., 2005; Liu et al., 2010) and coprecipitation (Lee et al., 2009; Dungkaew et al., 2012), the role of HAP in the immobilization of As should not be overestimated when HAP is converted from a precursor containing As. Furthermore, once MICP is used as an HM remediation technology, the long term stability of the HM-bearing $CaCO_3$ should be considered, especially in future geochemical conditions.

4. Conclusions

In this contribution, we investigated arsenic's fate during the conversion of bio-induced As-bearing $CaCO_3$ to HAP. We observed that calcite precipitated in the presence of As(III), while vaterite generated as well at a high concentration of As(V). After contacted with phosphate medium, most $CaCO_3$ converted to HAP, whose morphology changed from hexagonal to petal-like with the increase of arsenic concentration. Chemical analysis showed that the conversion process following MICP declined the As concentration in solid up to 88.19%, leading to an increase of 17.50% As concentration in the solution. Elemental mapping results showed that arsenic was homogeneously distributed in As-HAP. Moreover, HPLC-ICP-MS results confirmed the partial oxidation of As (III) to As(V) in calcite and HAP, suggesting these two phases favored the incorporation of arsenate. The discovery of As releasing during the conversion of As-$CaCO_3$ to HAP implies that As-bearing $CaCO_3$ is a possible new source of As pollution in a phosphorus-rich environment. Therefore, phosphatic fertilizer application should be more careful in As-contaminated calcareous soil.

CRediT authorship contribution statement

Maolin Wang: Investigation, Visualization, Writing - original draft. **Shijun Wu:** Conceptualization, Writing - review & editing, Supervision, Project administration, Funding acquisition. **Jianan Guo:** Investigation, Resources. **Zisheng Liao:** Investigation, Resources. **Yongqiang Yang:** Writing - review & editing. **Fanrong Chen:** Supervision, Funding acquisition. **Runliang Zhu:** Writing - review & editing, Funding acquisition.

Declaration of Competing Interest

The authors declare that they have no known competing financial interests or personal relationships that could have appeared to influence the work reported in this paper.

Acknowledgments

We are grateful for the financial support provided by the National Natural Science Foundation of China (Grant No. 41877135), Science and Technology Program of Guangzhou, China (Grant No. 201804020037), the Science and Technology Planning Project of Guangdong Province (Grant Nos. 2017B020236003 and 2020B1212060055) and the One-Three-Five Program of Guangzhou Institute of Geochemistry, Chinese Academy of Sciences (GIGCAS) (Grant No. 135PY201604). This is contribution No. IS-2976 from GIGCAS.

Appendix A. Supporting information

Supplementary data associated with this article can be found in the online version at doi:10.1016/j.jhazmat.2021.125261.

References

Achal, V., Pan, X., Fu, Q., Zhang, D., 2012. Biomineralization based remediation of As (III) contaminated soil by Sporosarcina ginsengisoli. J. Hazard. Mater. 201, 178–184.
Agency for toxic substance (ATSDR), 2019. ATSDR's 2019 Substance Priority List. https://www.atsdr.cdc.gov/spl/#2019spl.
Alexandratos, V.G., Elzinga, E.J., Reeder, R.J., 2007. Arsenate uptake by calcite: macroscopic and spectroscopic characterization of adsorption and incorporation mechanisms. Geochim. Cosmochim. Acta 71 (17), 4172–4187.
Andersen, F.A., Brecevic, L., Beuter, G., Dellamico, D.B., Calderazzo, F., Bjerrum, N.J., Underhill, A.E., 1991. Infrared spectra of amorphous and crystalline calcium carbonate. Acta Chem. Scand. 45 (10), 1018–1024.
Bardelli, F., Benvenuti, M., Costagliola, P., Di Benedetto, F., Lattanzi, P., Meneghini, C., Romanelli, M., Valenzano, L., 2011. Arsenic uptake by natural calcite: an XAS study. Geochim. Cosmochim. Acta 75 (11), 3011–3023.
Bates, M., Smith, A., Hopenhayn-Rich, C., 1992. Arsenic ingestion and internal cancers: a review. Am. J. Epidemiol. 135, 462–476.
Boquet, E., Boronat, A., Ramoscor, A., 1973. Production of calcite (calcium carbonate) crystals by soil bacteria is a general phenomenon. Nature 246 (5434), 527–529.
Borg, S., Liu, W., Pearce, M., Cleverley, J., MacRae, C., 2014. Complex mineral zoning patterns caused by ultra-local equilibrium at reaction interfaces. Geology 42 (5), 415–418.
Bothe, J.V., Brown, P.W., 1999. Arsenic immobilization by calcium arsenate formation. Environ. Sci. Technol. 33 (21), 3806–3811.
Bronick, C.J., Lal, R., 2005. Soil structure and management: a review. Geoderma 124 (1–2), 3–22.
Brüske-Hohlfeld, I., 2009. Environmental and occupational risk factors for lung cancer. In: Verma, M. (Ed.), Cancer Epidemiology. Methods in Molecular Biology, 472. Humana Press. https://doi.org/10.1007/978-1-60327-492-0_1.
Chakhmouradian, A.R., Reguir, E.P., Zaitsev, A.N., Coueslan, C., Xu, C., Kynicky, J., Mumin, A.H., Yang, P., 2017. Apatite in carbonatitic rocks: compositional variation, zoning, element partitioning and petrogenetic significance. Lithos 274, 188–213.
Chakraborty, S., Bardelli, F., Mullet, M., Greneche, J.-M., Varma, S., Ehrhardt, J.-J., Banerjee, D., Charlet, L., 2011. Spectroscopic studies of arsenic retention onto biotite. Chem. Geol. 281 (1–2), 83–92.
Christy, A.G., 2017. A review of the structures of vaterite: the impossible, the possible, and the likely. Cryst. Growth Des. 17 (6), 3567–3578.
Di Benedetto, F., Costagliola, P., Benvenuti, M., Lattanzi, P., Romanelli, M., Tanelli, G., 2006. Arsenic incorporation in natural calcite lattice: evidence from electron spin echo spectroscopy. Earth Planet. Sci. Lett. 246 (3–4), 458–465.
Dixit, S., Hering, J.G., 2003. Comparison of arsenic (V) and arsenic (III) sorption onto iron oxide minerals: implications for arsenic mobility. Environ. Sci. Technol. 37 (18), 4182–4189.
Dungkaew, W., Haller, K.J., Flood, A.E., Scamehorn, J.F., 2012. Arsenic removal by precipitation with calcium phosphate hydroxyapatite. Adv. Mater. Res. 506, 413–416.
Edmond, J.M., 1992. Himalayan tectonics, weathering processes, and the strontium isotope record in marine limestones. Science 258 (5088), 1594–1597.
Fernandez-Diaz, L., Fernandez-Gonzalez, A., Prieto, M., 2010. The role of sulfate groups in controlling CaCO3 polymorphism. Geochim. Cosmochim. Acta 74 (21), 6064–6076.
Fernandez-Gonzalez, A., Fernandez-Diaz, L., 2013. Growth of calcium carbonate in the presence of Se(VI) in silica hydrogel. Am. Miner. 98 (10), 1824–1833.
Fernández-Martínez, A., Román-Ross, G., Cuello, G.J., Turrillas, X., Charlet, L., Johnson, M.R., Bardelli, F., 2006. Arsenic uptake by gypsum and calcite: modelling and probing by neutron and X-ray scattering. Phys. B Condens. Matter 385–386, 935–937.
Fleet, M.E., Liu, X., 2008. Accommodation of the carbonate ion in fluorapatite synthesized at high pressure. Am. Miner. 93 (8–9), 1460–1469.
Garelick, H., Jones, H., Dybowska, A., Valsami-Jones, E., 2008. Arsenic pollution sources. Rev. Environ. Contam. Toxicol. 197, 17–60.
Gat, D., Ronen, Z., Tsesarsky, M., 2017. Long-term sustainability of microbial-induced CaCO3 precipitation in aqueous media. Chemosphere 184, 524–531.
Grasby, S.E., 2003. Naturally precipitating vaterite (μ-CaCO3) spheres: unusual carbonates formed in an extreme environment. Geochim. Cosmochim. Acta 67 (9), 1659–1666.
Hughes, M.F., Beck, B.D., Yu, C., Lewis, A.S., Thomas, D.J., 2011. Arsenic exposure and toxicology: a historical perspective. Toxicol. Sci. 123 (2), 305–332.
Juillot, F., Ildefonse, P., Morin, G., Calas, G., de Kersabiec, A.M., Benedetti, M., 1999. Remobilization of arsenic from buried wastes at an industrial site: mineralogical and geochemical control. Appl. Geochem. 14 (8), 1031–1048.
Kabalah-Amitai, L., Mayzel, B., Kauffmann, Y., Fitch, A.N., Bloch, L., Gilbert, P.U., Pokroy, B., 2013. Vaterite crystals contain two interspersed crystal structures. Science 340 (6131), 454–457.
Kamiya, N., Kagi, H., Tsunomori, F., Tsuno, H., Notsu, K., 2004. Effect of trace lanthanum ion on dissolution and crystal growth of calcium carbonate. J. Cryst. Growth 267 (3–4), 635–645.
Katsikopoulos, D., Fernandez-Gonzalez, A., Prieto, A.C., Prieto, M., 2008. Co-crystallization of Co(II) with calcite: implications for the mobility of cobalt in aqueous environments. Chem. Geol. 254 (1–2), 87–100.
Khairul, I., Wang, Q.Q., Jiang, Y.H., Wang, C., Naranmandura, H., 2017. Metabolism, toxicity and anticancer activities of arsenic compounds. Oncotarget 8 (14), 23905–23926.
Kirsch, K., Navarre-Sitchler, A.K., Wunsch, A., McCray, J.E., 2014. Metal release from sandstones under experimentally and numerically simulated CO_2 leakage conditions. Environ. Sci. Technol. 48 (3), 1436–1442.
Kumari, D., Qian, X.-Y., Pan, X., Achal, V., Li, Q., Gadd, G.M., 2016. Microbially-induced carbonate precipitation for immobilization of toxic metals. In: Sariaslani, S., Gadd, G.M. (Eds.), Advances in Applied Microbiology, 94, 79–108.
Lee, Y.J., Stephens, P.W., Tang, Y., Li, W., Phillips, B.L., Parise, J.B., Reeder, R.J., 2009. Arsenate substitution in hydroxylapatite: structural characterization of the Ca5 (PxAs1-xO4)3OH solid solution. Am. Miner. 94 (5–6), 666–675.
Liu, G., Talley, J.W., Na, C.Z., Larson, S.L., Wolfe, L.G., 2010. Copper doping improves hydroxyapatite sorption for arsenate in simulated groundwaters. Environ. Sci. Technol. 44 (4), 1366–1372.
Liu, W., Mei, Y., Etschmann, B., Brugger, J., Pearce, M., Ryan, C.G., Borg, S., Wykes, J., Kappen, P., Paterson, D., 2017. Arsenic in hydrothermal apatite: oxidation state, mechanism of uptake, and comparison between experiments and nature. Geochim. Cosmochim. Acta 196, 144–159.
Maravelaki-Kalaitzaki, P., 2005. Black crusts and patinas on pentelic marble from the Parthenon and Erechtheum (Acropolis, Athens): characterization and origin. Anal. Chim. Acta 532 (2), 187–198.
Neto, A.S., Ferreira, J.M.F., 2018. Synthetic and marine-derived porous scaffolds for bone tissue engineering. Materials 11 (9), 1702.
Onac, B.P., 2019. Minerals in caves. In: White, W.B., Pipan, T., Culver, D.C. (Eds.), Encyclopedia of Caves, third edition.,. Academic Press, pp. 699–709.
Palmer, M.R., Edmond, J.M., 1993. Uranium in river water. Geochim. Cosmochim. Acta 57 (20), 4947–4955.
Pan, Y.M., Fleet, M.E., 2002. Compositions of the apatite-group minerals: substitution mechanisms and controlling factors. Rev. Miner. Geochem 48, 13–49.
Pedrosa, E.T., Putnis, C.V., Putnis, A., 2016. The pseudomorphic replacement of marble by apatite: the role of fluid composition. Chem. Geol. 425, 1–11.
Phillips, A.J., Gerlach, R., Lauchnor, E., Mitchell, A.C., Cunningham, A.B., Spangler, L., 2013. Engineered applications of ureolytic biomineralization: a review. Biofouling 29 (6), 715–733.
Putnis, A., 2009. Mineral replacement reactions. Rev. Mineral. Geochem. 70 (1), 87–124.
Puzio, B., Manecki, M., Kwasniak-Kominek, M., 2018. Transition from endothermic to exothermic dissolution of hydroxyapatite $Ca_5(PO_4)_3OH$–Johnbaumite $Ca_5(AsO_4)_3OH$ solid solution series at temperatures ranging from 5 to 65 °C. Minerals 8 (7), 281.
Redman, A.D., Macalady, D.L., Ahmann, D., 2002. Natural organic matter affects arsenic speciation and sorption onto hematite. Environ. Sci. Technol. 36 (13), 2889–2896.
Renard, F., Putnis, C.V., Montes-Hernandez, G., Ruiz-Agudo, E., Hovelmann, J., Sarret, G., 2015. Interactions of arsenic with calcite surfaces revealed by in situ nanoscale imaging. Geochim. Cosmochim. Acta 159, 61–79.
Ripamonti, U., Crooks, J., Khoah, L., Roden, L., 2009. The induction of bone formation by coral-derived calcium carbonate/hydroxyapatite constructs. Biomaterials 30 (7), 1428–1439.
Román-Ross, G., Cuello, G.J., Turrillas, X., Fernández-Martínez, A., Charlet, L., 2006. Arsenite sorption and co-precipitation with calcite. Chem. Geol. 233 (3), 328–336.
Romero, F., Armienta, M., Carrillo-Chavez, A., 2004. Arsenic sorption by carbonate-rich aquifer material, a control on arsenic mobility at Zimapan, Mexico. Arch. Environ. Contam. Toxicol. 47 (1), 1–13.
Roy, P., Saha, A., 2002. Metabolism and toxicity of arsenic: a human carcinogen. Curr. Sci. 38–45.
Sadiq, M., 1997. Arsenic chemistry in soils: an overview of thermodynamic predictions and field observations. Water Air Soil Pollut. 93 (1–4), 117–136.
Sanchez-Pastor, N., Gigler, A.M., Cruz, J.A., Park, S.H., Jordan, G., Fernandez-Diaz, L., 2011. Growth of calcium carbonate in the presence of Cr(VI). Cryst. Growth Des. 11 (7), 3081–3089.
Sassoni, E., Naidu, S., Scherer, G.W., 2011. The use of hydroxyapatite as a new inorganic consolidant for damaged carbonate stones. J. Cult. Herit. 12 (4), 346–355.
Sassoni, E., Graziani, G., Franzoni, E., 2015. Repair of sugaring marble by ammonium phosphate: comparison with ethyl silicate and ammonium oxalate and pilot application to historic artifact. Mater. Des. 88, 1145–1157.
Sato, M., Matsuda, S., 1969. Structure of vaterite and infrared spectra. Z. Krist. Cryst. Mater. 129 (5–6), 405–410.
Schnug, E., Jacobs, F., Stöven, K., 2018. Guano: the white gold of the seabirds. In: Mikkola, H. (Ed.), Seabirds. IntechOpen, pp. 81–100.

Shen, J., Yuan, L., Zhang, J., Li, H., Bai, Z., Chen, X., Zhang, W., Zhang, F., 2011. Phosphorus dynamics: from soil to plant. Plant Physiol. 156 (3), 997–1005.
Smedley, P.L., Kinniburgh, D., 2002. A review of the source, behaviour and distribution of arsenic in natural waters. Appl. Geochem. 17 (5), 517–568.
Sneddon, I.R., Garelick, H., Valsami-Jones, E., 2005. An investigation into arsenic(V) removal from aqueous solutions by hydroxylapatite and bone-char. Mineral. Mag. 69 (5), 769–780.
Spear, F.S., Pyle, J.M., 2002. Apatite, monazite, and xenotime in metamorphic rocks. Rev. Mineral. Geochem. 48 (1), 293–335.
Vazquez-Calvo, C., Alvarez de Buergo, M., Fort, R., 2006. Patinas in the architectural heritage of Lerma, Burgos (Spain). Proceedings of the International Conference on Heritage, Weathering and Conservation, HWC 2, 969–974.
Wang, Y.-Y., Chai, L.-Y., Yang, W.-C., 2019a. Arsenic distribution and pollution characteristics. In: Chai, L.Y. (Ed.), Arsenic Pollution Control in Nonferrous Metallurgy. Springer, Singapore, pp. 1–15.
Wang, M., Wu, S., Guo, J., Zhang, X., Yang, Y., Chen, F., Zhu, R., 2019b. Immobilization of cadmium by hydroxyapatite converted from microbial precipitated calcite. J. Hazard. Mater. 366, 684–693.
WHO, 2001. Arsenic and arsenic compounds. Environmental Health Criteria 224, second ed. World Health Organization, Geneva.
Wilson, S.C., Lockwood, P.V., Ashley, P.M., Tighe, M., 2010. The chemistry and behaviour of antimony in the soil environment with comparisons to arsenic: a critical review. Environ. Pollut. 158 (5), 1169–1181.
Wunsch, A., Navarre-Sitchler, A.K., Moore, J., McCray, J.E., 2014. Metal release from limestones at high partial-pressures of CO_2. Chem. Geol. 363, 40–55.
Xia, X., Ji, J., Yang, Z., Han, H., Huang, C., Li, Y., Zhang, W., 2020. Cadmium risk in the soil-plant system caused by weathering of carbonate bedrock. Chemosphere 254, 126799.
Yokoyama, Y., Tanaka, K., Takahashi, Y., 2012. Differences in the immobilization of arsenite and arsenate by calcite. Geochim. Cosmochim. Acta 91, 202–219.
Zhang, D.N., Wang, S.F., Wang, Y., Gomez, M.A., Jia, Y.F., 2019. The long-term stability of calcium arsenates: implications for phase transformation and arsenic mobilization. J. Environ. Sci. 84, 29–41.